PHYSICAL REVIEW B **81**, 205304 (2010)

Theoretical study of nuclear spin polarization and depolarization in self-assembled quantum dots

Chia-Wei Huang and Xuedong Hu
Department of Physics, University at Buffalo–The State University of New York, Buffalo, New York 14260-1500, USA

(Received 20 January 2010; published 4 May 2010)

We investigate how the strain-induced nuclear quadrupole interaction influences the degree of nuclear spin polarization driven by optical pumping in self-assembled quantum dots. Our calculation shows that the achievable nuclear spin polarization in $\mathrm{In}_x\mathrm{Ga}_{1-x}\mathrm{As}$ quantum dots is related to the concentration of indium and the resulting strain distribution in the dots. The interplay between the nuclear quadrupole interaction and Zeeman splitting leads to interesting features in the magnetic field dependence of the nuclear spin polarization. Our results are in qualitative agreement with measured nuclear spin polarization by various experimental groups.

DOI: 10.1103/PhysRevB.81.205304 PACS number(s): 85.35.Be, 76.60.−k, 03.67.Lx

I. INTRODUCTION

Nuclear spin dynamics has been studied extensively in many fields.[1,2] In recent years, nuclear spin dynamics in semiconductor quantum dots has attracted intense interest because of the excellent quantum coherence properties of nuclear spins. Indeed, nuclear spins in nanostructures have been suggested as qubits for a quantum computer[3] and for use as quantum memory.[4] For either purpose, high degree of nuclear spin polarization (NSP) is a prerequisite.

Nuclear spins in nanostructures also form an important environment for electron spins, which have been proposed as a candidate for qubits.[5] Through the hyperfine interaction the nuclear spins create a spatially and temporally fluctuating magnetic field for the electron spins, which leads to spin decoherence.[6–12] It has been suggested theoretically that such decoherence could potentially be suppressed if nuclear spin fluctuations are suppressed,[13–15] and one way to realize such suppression is via dynamic nuclear spin polarization. Furthermore, the coupled electron-nuclear spin problem is an intriguing example of a quantum many-body problem, and is still not solved completely.

Dynamic NSP (DNSP) has been studied for many decades.[16] It has been demonstrated in semiconductor quantum wells[17–19] and quantum dots[20–26] through a variety of experiments. Physically, DNSP can be achieved either electrically or optically, where a pumped electron can transfer its spin polarization to nuclear spins via the contact hyperfine interaction. A range of values for nuclear spin polarization has been reported by several experimental groups. For example, using electrically controlled DNSP, Petta *et al.*[24] reported approximately 1% NSP in lateral coupled GaAs double quantum dots; while Baugh *et al.*[22] reported 40% NSP in vertical coupled GaAs quantum dots with 5% In. With optically pumped DNSP, Gammon *et al.*[20] reported 60% NSP in interface fluctuation GaAs quantum dots, while recent experiments have achieved NSP in $\mathrm{In}_x\mathrm{Ga}_{1-x}\mathrm{As}$ self-assembled quantum dots at various magnetic fields. In particular, approximately 10–20 % of NSP is created in $\mathrm{In}_{0.9}\mathrm{Ga}_{0.1}\mathrm{As}$ quantum dots <1 T,[23] 40% in $\mathrm{In}_{0.6}\mathrm{Ga}_{0.4}\mathrm{As}$ at around 2 T,[27–29] and 80% in $\mathrm{In}_{0.9}\mathrm{Ga}_{0.1}\mathrm{As}$ at 5 T.[30] It is evident that the experimental results vary greatly as experimental conditions and physical systems are varied. So far there has been no systematic theoretical studies of NSP and how it depends on the various system parameters such as applied field and material composition.

In this paper we study dynamic nuclear spin polarization in $\mathrm{In}_x\mathrm{Ga}_{1-x}\mathrm{As}$ quantum dots via optical pumping of confined electrons. These self-assembled dots are generally highly strained and we are particularly interested in the NSP of these dots in different strain environments. Specifically, the strain breaks the cubic symmetry of the crystal lattice and creates an electric field gradient which couples to the nuclear quadrupole moment,[31] which in turn leads to mixing of nuclear spin eigenstates. We use a simplified model of the quantum dot where the electric field gradient is axially symmetric. We first study how the As NSP responds to various strain strengths, angles, and cotunneling constants in magnetic fields. For the electron-nuclear spin transfer, we consider both phonon-assisted and cotunneling-assisted spin flip processes. Lastly, we consider NSP of $\mathrm{In}_x\mathrm{Ga}_{1-x}\mathrm{As}$ quantum dots with different compositions.

The paper is organized as follows. We describe the scheme of DNSP in Sec. II and our model Hamiltonian in Sec. III. We show our results of nuclear spin polarization in As nuclei and in different compositions of $\mathrm{In}_x\mathrm{Ga}_{1-x}\mathrm{As}$ quantum dots at various magnetic fields in Sec. IV. We discuss some interesting features related to our calculation in Sec. V. Finally, we summarize our results in Sec. VI and draw our conclusions.

II. SCHEME OF NUCLEAR SPIN POLARIZATION

$\mathrm{In}_x\mathrm{Ga}_{1-x}\mathrm{As}$ self-assembled quantum dots (SAQDs) are formed by a strain-driven process, where the strain arises from the lattice mismatch between the InAs deposition layers and the GaAs substrate. The strain in the QDs breaks the lattice symmetry and creates electric field gradients in the dots. The shape of $\mathrm{In}_x\mathrm{Ga}_{1-x}\mathrm{As}$ QDs varies among experiments, ranging from pancakelike to pyramidlike and domelike. The resulting distribution of electric field gradients thus also differs from dot to dot. Even in the same dot, the strain distribution is not uniform. For example, the strain at the edge of a quantum dot is generally larger than at the center of the dot.[32] Therefore, nuclear spins in different regions of a QD experience electric field gradients of different strengths and directions. For an estimate of NSP, we start with a simplified model of a pancakelike cylindrically symmetric QD as shown in Fig. 1. The electric field gradients in such a dot are thus axially symmetric. The largest electric field gradient V_{ZZ} is along the principal axis Z, which is defined to be

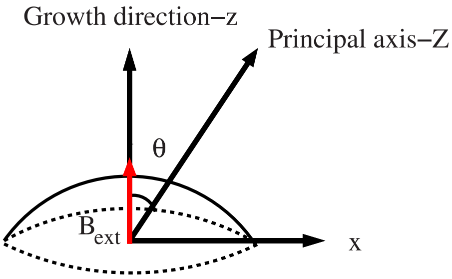

FIG. 1. (Color online) A model of a self-assembled quantum dot. We assume the field gradients in the self-assembled quantum dot are axially symmetric. The largest electric field gradient component V_{ZZ} is along the principal axis Z, which deviates from the growth direction (the z axis) by an angle θ. The external magnetic field is assumed to be along the z axis.

normal to the pancake surface. For instance, for a lattice site in the xz plane, Z would be in the xz plane as well, and deviates from the growth direction (the z axis) by an angle of θ.

We base our calculation on the experimental conditions in Refs. 27, 28, 33, and 34 (see Fig. 2), where the SAQD is embedded in a Schottky diode heterostructure, so that the charged states of the QD can be controlled. In addition, the gate voltage can be tuned to allow zero or one charge (electron or hole) on the dot.

In such a system dynamic nuclear spin polarization is realized via optical pumping. A circularly polarized photon creates an electron-hole pair, which is then captured in the QD as a negative trion,[24,34] neutral exciton,[33] or positive trion.[26–29] When the QD contains one electron, this electron is likely spin polarized and can polarize a nuclear spin through the hyperfine interaction. The probability to realize this spin transfer process depends on the experimental conditions, such as the type of excitation used (pulsed or cw) and the initial charged states in the quantum dot (X^0, X^-, or X^+). Therefore, an experimentally determined factor f_e is used to modify the electron-nuclear spin-transfer probability (see Sec. III C).

In a finite magnetic field the hyperfine-mediated transfer of polarization from the electron spin to the nuclear spins has to be assisted by another process because of the large mismatch of the electron and nuclear Zeeman energies. In our case we consider phonon-assisted and tunneling-assisted processes. More specifically, in the Schottky-diode configuration the confined electron can flip its spin via cotunneling to the external reservoir (For details see Sec. III C 1). This cotunneling-assisted spin-flip process is efficient at low magnetic fields. In the high-field regions (or in an isolated QD), the electron-phonon interaction provides the more efficient channel to compensate for the energy mismatch between electron and nuclear spins. (For details see Sec. III C 2.)

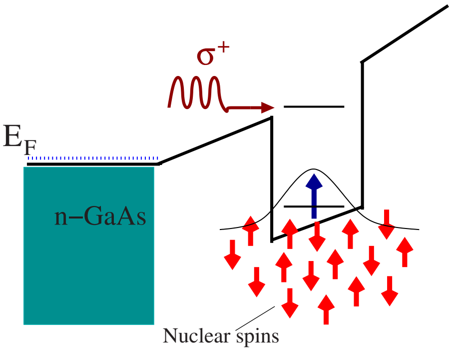

FIG. 2. (Color online) Schematic of the setup for a typical optical orientation experiment (Refs. 33 and 34) The self-assembled quantum dot is embedded in a Schottky diode heterostructure, where the gate voltage is tuned to allow only one-electron orbital state below the Fermi level. Nuclear spins are polarized by an optically pumped electron captured in the quantum dot.

III. MODEL HAMILTONIAN

The total Hamiltonian for the nuclear spin polarization scheme we consider is given as follows:

$$H_{tot} = H_n + H_e + H_{hf},$$

where H_n is the Hamiltonian for the nuclear spins in the quantum dot, H_e is for the electron spin, and H_{hf} is the hyperfine interaction between the electron and nuclear spins. Below we describe each of the terms in H_{tot} in detail and discuss the role they play in the DNSP process.

A. Hamiltonian of nuclear spin in quantum dots

In the presence of an external magnetic field (along the z axis, which is the growth direction), the effective Hamiltonian of nuclear spins in our simplified model of a quantum dot (see Fig. 1) consists of three main parts: Zeeman splitting, the nuclear electric quadrupole interaction, and nuclear spin dipolar interactions,

$$H_n = H_z^n + H_Q + H_d, \tag{1}$$

where

$$H_z^n = \sum_{i=1}^{N} \hbar\gamma B_z I_z^i,$$

$$H_Q = \sum_{i=1}^{N} \frac{eQV_{ZZ}^i}{4I(2I-1)}[3(I_Z^i)^2 - I(I+1)],$$

$$H_d = \sum_{i<j}^{N} \frac{\mu_0\hbar^2\gamma^2}{4\pi}\left[\frac{\mathbf{I}^i\cdot\mathbf{I}^j}{R_{ij}^3} - \frac{3(\mathbf{I}^i\cdot\mathbf{R}_{ij})(\mathbf{I}^j\cdot\mathbf{R}_{ij})}{R_{ij}^5}\right].$$

H_z^n represents the nuclear Zeeman energy (E_z^n), where I_z is the projection of a nuclear spin along the external magnetic field and γ is the nuclear gyromagnetic ratio (see Table I).

H_Q represents the electric quadrupole interaction (E_Q),[1,2] through which the nuclear spins in an $In_xGa_{1-x}As$ SAQD couple to the electric field gradients in the crystal lattice. The asymmetric part of the quadrupole interaction is neglected here because we assume a pancake-shaped QD, where $V_{ZZ} \gg V_{XX}, V_{YY}$. Q is the electric quadrupole moment of a nucleus and e is the elementary charge. V_{ZZ} is the electric field gradient along the principal axis Z. $V_{ZZ}=S_{11}e_{ZZ}$,[31] where the constant S_{11} is experimentally determined (see in Table I)

TABLE I. Material parameters used in our calculation. Nuclear electric quadrupole moment Q and constant S_{11} (which relates electric field gradient to strain) are taken from Refs. 35 and 36. Nuclear spin gyromagnetic ratios are taken from Ref. 37.

Elements	In	Ga	As
Nuclear spin I	9/2	3/2	3/2
Electric quadrupole moment Q (10^{-24} cm^2)	0.86	0.27	0.2
S_{11} (10^{15} statcoulombs/cm^3)	16.7	9.1	13
Gyromagnetic ratio γ (μeV/T)	0.039	0.042	0.03
Hyperfine constant A (μeV)	56	42	46

and e_{ZZ} is the Z component of the strain tensor, which is approximately 4–8 % for In$_x$Ga$_{1-x}$As QDs with different compositions.[32,38–42] The electric field gradients introduced by charged states in the QD (Ref. 43) are at least two orders of magnitude smaller than the electric field gradient caused by the broken symmetry of the crystal lattice, therefore we exclude the effect of the former.

H_d represents the dipolar interaction between different nuclear spins, where R_{jk} is the distance between the ith and the jth the nucleus, μ_0 is the free space permeability. The local field B_{loc} that this dipolar coupling produces is around 1 G and the dynamical effect of the dipolar interaction is nuclear spin diffusion. In our calculation, we do not deal with the case when the external magnetic field is smaller than the local field (the smallest external field we use is 10 mT). Furthermore, nuclear spin diffusion is strongly suppressed in a small QD,[44] and its time scale (tens of seconds to minutes[45]) is much longer than the time scale of DNSP in our study. Therefore we exclude H_d in our calculation. Since H_d is the only direct interaction between nuclear spins, its removal significantly simplifies our study: the nuclear spins can now be treated independently from each other. The hyperfine-mediated nuclear spin interaction[9,46,47] is also neglected in our calculation, as the hyperfine interaction is only turned on randomly for a small fraction of time in experiments, as we will discuss in Sec. III C.

The nuclear spin Hamiltonian is thus simplified as

$$H_n = \hbar\gamma B_z I_z + \frac{eQV_{ZZ}}{4I(2I-1)}\left[I_Z^2 - \frac{1}{3}I(I+1)\right].$$

In our simplified model of the quantum dot, the principal axis Z for the largest electric field gradient V_{ZZ} deviates from the z axis by an angle θ and I_Z is the projection of a nuclear spin along the principal axis Z. For a pancake-shaped QD, the angle θ is generally quite small. Therefore, while for all the calculations presented in this paper we treat the nuclear spin Hamiltonian (1) exactly, for the qualitative discussion in Sec. IV we take a small-angle approximation and simplify Hamiltonian (1). For example, in the case of $I=3/2$ we obtain,

$$H_z^n + H_Q = \begin{array}{c} \begin{array}{cccc} I_z=\frac{3}{2} & I_z=\frac{1}{2} & I_z=-\frac{1}{2} & I_z=-\frac{3}{2} \end{array} \\ \begin{pmatrix} \frac{3}{2}E_z^n + E_Q' & \sqrt{3}E_Q\theta & \frac{\sqrt{3}}{2}E_Q\theta^2 & 0 \\ \sqrt{3}E_Q\theta & \frac{1}{2}E_z^n - E_Q' & 0 & \frac{\sqrt{3}}{2}E_Q\theta^2 \\ \frac{\sqrt{3}}{2}E_Q\theta^2 & 0 & -\frac{1}{2}E_z^n - E_Q' & -\sqrt{3}E_Q\theta \\ 0 & \frac{\sqrt{3}}{2}E_Q\theta^2 & -\sqrt{3}E_Q\theta & -\frac{3}{2}E_z^n + E_Q' \end{pmatrix} \end{array}, \tag{2}$$

where $E_Q' = E_Q(3\cos^2\theta - 1)/2 \approx E_Q$. When the off-diagonal terms in Eq. (2) are small compared to the diagonal terms, we can construct the new eigenstates perturbatively. In a nondegenerate case, the nuclear spin eigenstates are as follows:

$$|1\rangle = \left|+\frac{3}{2}\right\rangle + a\left|+\frac{1}{2}\right\rangle + b\left|-\frac{1}{2}\right\rangle,$$

$$|2\rangle = \left|+\frac{1}{2}\right\rangle - a\left|+\frac{3}{2}\right\rangle + c\left|-\frac{3}{2}\right\rangle,$$

$$|3\rangle = \left|-\frac{1}{2}\right\rangle - b\left|+\frac{3}{2}\right\rangle - d\left|-\frac{3}{2}\right\rangle,$$

$$|4\rangle = \left|-\frac{3}{2}\right\rangle + c\left|+\frac{1}{2}\right\rangle + d\left|-\frac{1}{2}\right\rangle, \tag{3}$$

where $a=\sqrt{3}E_Q\theta/(E_z^n+2E_Q)$, $b=\sqrt{3}E_Q\theta^2/4(E_z^n+E_Q)$, $c=\sqrt{3}E_Q\theta^2/4(E_z^n-E_Q)$, and $d=\sqrt{3}E_Q\theta/(E_z^n-2E_Q)$. For a degenerate case as shown in Figs. 3(b) and 3(c), the eigenstates have to be solved by directly diagonalizing the Hamiltonian

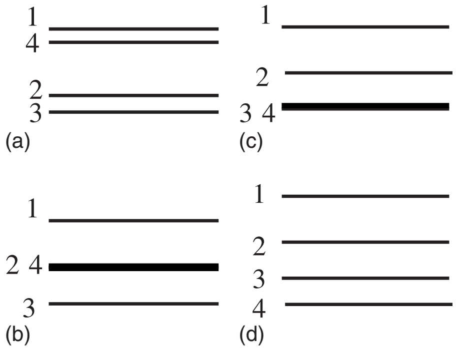

FIG. 3. Sketches of the energy-level diagram of a single nuclear spin (not to scale). Due to the presence of the quadrupole interaction, the eigenstates are generally no longer the eigenvectors of I_z. We label the real eigenstates as ($|1\rangle$, $|2\rangle$, $|3\rangle$, and $|4\rangle$), which are combinations of I_z eigenstates with $m_z=\{\frac{3}{2},\frac{1}{2},-\frac{1}{2},-\frac{3}{2}\}$. (a) Low-field situations, when the quadrupole interaction (E_Q) is stronger than the nuclear Zeeman effect (E_z^n). (b) 2–4 degeneracy, when the quadrupole interaction and nuclear Zeeman energy are resonant ($E_z^n=E_Q$). (c) 3–4 degeneracy, when $E_z^n=2E_Q$. (d) High magnetic field region, when the Zeeman energy is dominant, and the quadrupole interaction is negligible.

in Eq. (2). Taking the state 2–4 degeneracy, for example, one would expect a complete mixing between state 2 and state 4.

B. Hamiltonian of electron spin in quantum dots

The effective Hamiltonian of the electron in the quantum dot consists of three main parts: Zeeman splitting, tunnel coupling to the external reservoir, and the electron-phonon interaction,

$$H_e = H_z^e + H_T + H_{ep},$$

where

$$H_z^e = - g^* \mu_B B_z S_z,$$

$$H_T = \sum_{k\sigma} \varepsilon_k n_{k\sigma} + \varepsilon_0 \sum_{\sigma} n_\sigma + U n_\uparrow n_\downarrow + \sum_{k\sigma} V_k (c_{k\sigma}^\dagger c_\sigma + c_\sigma^\dagger c_{k\sigma}), \tag{4}$$

$$H_{ep} = \sum_{q\nu} M_{q\nu} (a_{-q\nu}^\dagger + a_{q\nu}) \exp(i\mathbf{q}\cdot\mathbf{r}).$$

Here H_z^e represents the electron Zeeman energy, where g^* is the electron effective g factor in In$_x$Ga$_{1-x}$As QDs, μ_B is the Bohr magneton, and S_z is the z component of the electron spin operator. H_T is the Anderson Hamiltonian,[48–50] suitable for describing the experimental setup in our consideration (see Fig. 2), where a QD is tunnel coupled to the outside Fermi sea. In Eq. (4), $c^\dagger$ and c represent electron creation and annihilation operators, and n the number operators. We describe a reservoir state with index k, energy ε_k, and electron spin index σ. The single electron energy level in the quantum dot is ε_0. U is the on-site Coulomb interaction and V_k is the tunneling matrix element. H_{ep} represents the electron-phonon coupling, where $a_{-q\nu}^\dagger$ and $a_{q\nu}$ represent phonon creation and annihilation operators, with quasimomentum q and branch index ν. We consider both the deformation potential and piezoelectric potential in $M_{q\nu}$.[50]

C. Hyperfine interaction

In our scheme, NSP is pumped by optically oriented electrons via the contact hyperfine interaction,

$$H_{hf}(t) = h(t) \sum_{k}^{N} A|\Phi(R_k)|^2 \times \left[I_z^k S_z + \frac{1}{2}(I_+^k S_- + I_-^k S_+) \right], \tag{5}$$

where A is the hyperfine coupling constant (see Table I). N is approximately 10^4 in an In$_x$Ga$_{1-x}$As SAQD. $\Phi(R_k)$ is the electron wave function at the kth nucleus site, which is Gaussian for harmonic confinement. For our calculations presented in this paper, we take $|\Phi(R_k)|^2$ as $1/N$, effectively assuming a constant electron wave function in the QD. This assumption makes the definition of nuclear spin polarization well defined, while in the case of a Gaussian wave function the calculation of overall NSP depends on where the dot is truncated, as the edge of the dot would generally be only slightly polarized. $h(t)$ is a random function depending on the experimental procedures and conditions. While we are not going to describe the full details of each pumping scheme, the nature of $h(t)$ depends on whether the system is in the trion or neutral exciton regime. For example, for the X^+ scheme, $h(t)$ is dependent on the trapping and recombination of the electron;[27] while for X^- scheme it is dependent on the exciton recombination and electron tunneling time;[34,51] and for X^0 it is dependent on the exciton recombination time.[33] The fraction f_e is defined as the mean value of this temporal function $h(t)$, and it represents the fraction of the time when only one electron is left in the quantum dot and the hyperfine interaction is "turned on," so that the electron-nuclear spin flip flop can be realized. We use 0.035 for f_e in our calculations based on experimental observations.[51] The small value of f_e, together with the fact that $h(t)$ is random in time to a degree, justify our approximation of neglecting higher-order effects of the hyperfine interaction throughout our calculations.

Depending on the helicity of the optical excitation (σ^+/σ^-) relative to the applied external magnetic field, and through the flip-flop terms in the hyperfine interaction, the electron can pump nuclear spins either to the highest-energy spin state or the lowest-energy state. These spin flip flops are responsible for pumping the nuclear spins in the NSP process (blue one-way arrows in Fig. 5). In Secs. III C 1 and III C 2 we calculate the pumping rates based on the specific physical processes involved.

1. Cotunneling-assisted spin-flip processes

The electron spin in the QD can interact with an electron spin in the Fermi sea via cotunneling processes so that the electron Zeeman levels are broadened. The spin-flip probability and level broadening can be calculated applying Schrieffer-Wolf transformation to Eq. (4).[48,49,52,53] For each Zeeman level,

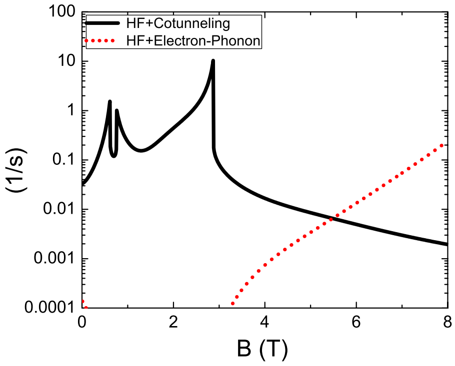

FIG. 4. (Color online) Comparison of cotunneling-assisted nuclear spin pumping rates with phonon-assisted rates. Here the Overhauser field is antiparallel to the external magnetic field and the angle between the largest electric field gradient and the external magnetic field is 2° (we use these conditions in the following figures, unless otherwise noted). The cotunneling-assisted spin-flip process is more efficient at low to intermediate magnetic fields ($B < 5$ T). For higher fields, the phonon-assisted spin-flip process is more efficient.

$$\rho(\varepsilon_i) = \frac{1}{2\pi}\frac{\Gamma_c}{(\varepsilon_i - \varepsilon_0)^2 + \Gamma_c^2/4},$$

where Γ_c is the level broadening due to the cotunneling processes.

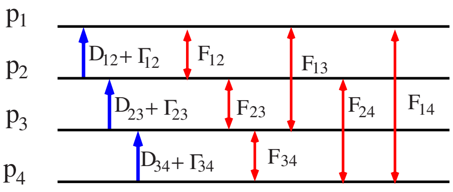

FIG. 5. (Color online) Transitions induced by the hyperfine interaction among nuclear spin states with $I=3/2$. The blue one-way arrows represent the transitions induced by the flip-flop terms in Eq. (5) and are responsible for pumping of the nuclear spins by the trapped electron spin. For an open-dot system as shown in Fig. 2, the cotunneling-assisted spin-flip rate D is dominant at low to intermediate magnetic fields. At high fields or in an isolated dot, the phonon-assisted pumping rate Γ^{ph} is dominant. The red two-way arrows represent transitions due to the mixture of different nuclear spin states, which originate from the I_zS_z term in Eq. (5). These processes are responsible for depolarization.

The probability of electron-nuclear spin flip-flop processes increases when the overlap between the two broadened electron Zeeman states increases. Therefore the cotunneling-assisted spin flip flop is more important at low magnetic fields. The transition rate between an initial state $|\uparrow i\rangle$ and a final state $|\downarrow j\rangle$ can be calculated with the Fermi's golden rule as,

$$\begin{aligned} D_{i,j} &= \frac{2\pi}{\hbar} f_e \left(\frac{A}{N}\right)^2 |\langle \downarrow j|I_+S_-|\uparrow i\rangle|^2 \\ &\quad \times \int \rho(\varepsilon_i)\rho(\varepsilon_f)\,\delta(\varepsilon_f - \varepsilon_i - \Delta E)\,d\varepsilon_i d\varepsilon_f \\ &\approx \left(\frac{A}{N}\right)^2 \frac{2 f_e \tau_c |\langle \downarrow j|I_+S_-|\uparrow i\rangle|^2}{\hbar^2 + \tau_c^2(-g^*\mu_B B_z + \delta_n)^2}, \end{aligned} \tag{6}$$

where $\delta_n = 2A\langle I_z\rangle$ stands for the Overhauser shift and the + sign in front of the Overhauser field is due to our choice here that the external magnetic field is antiparallel to the Overhauser field. For parallel fields, $-\delta_n$ should be used. The correlation time, $\tau_c = 1/\Gamma_c$, describes the broadening of QD electron states due to cotunneling processes. It is estimated for a typical Schottky structure to be ~20 ns.[48] At low to intermediate magnetic fields, the cotunneling-assisted spin-flip processes are the most efficient in building up NSP in the QD, as shown in Fig. 4.

2. *Phonon-assisted spin-flip processes*

For an isolated dot, or a dot described in 1 in higher field regions, the cotunneling-assisted spin-flip processes become less efficient due to the larger electronic Zeeman splitting. Now the phonon-assisted spin-flip processes give the most efficient DNSP channel. The pumping rates due to the phonon-assisted spin-flip processes are

$$\begin{aligned} \Gamma_{i,j}^{ph} &= \frac{2\pi}{\hbar}\sum_{q\nu} |T_{ep}|^2 \times [\bar{n}_{q\nu}\delta(\hbar s q - E_z^e) + (\bar{n}_{q\nu}+1)\delta(E_z^e + \hbar s q)] \\ &= N_q[f_{def}(E_z^e) + f_{piezo}(E_z^e)], \end{aligned}$$

where

$$T_{ep} = \sum_{l\neq m} \frac{\langle m\downarrow j|H_{hf}|l\uparrow i\rangle\langle l|H_{ep}|m\rangle}{E_m - E_l + E_z^e} + \frac{\langle m|H_{ep}|l\rangle\langle l\downarrow j|H_{hf}|m\uparrow i\rangle}{E_m - E_l - E_z^e},$$

$$\begin{aligned} f_{def}(E_z^e) &\approx \frac{l_0^2}{24\pi}\frac{\Xi^2 f_e}{\rho s}\left(\frac{A}{N}\right)^2 \frac{(E_z^e)^5}{(\hbar s)^6} |\langle\downarrow j|I_+S_-|\uparrow i\rangle|^2 \\ &\quad \times \left\{\left[\frac{1}{\hbar\Omega_-}\left(1+\frac{E_z^e}{\hbar\Omega_-}\right) + \frac{1}{\hbar\Omega_+}\left(1-\frac{E_z^e}{\hbar\Omega_+}\right)\right]^2 \right. \\ &\quad \left. + \left[\frac{1}{\hbar\Omega_+}\left(1+\frac{E_z^e}{\hbar\Omega_+}\right) + \frac{1}{\hbar\Omega_-}\left(1-\frac{E_z^e}{\hbar\Omega_-}\right)\right]^2\right\}, \end{aligned}$$

$$\begin{aligned} f_{piezo}(E_z^e) &\approx \frac{l_0^2}{30\pi}\frac{(ee_{14})^2 f_e}{\rho s}\left(\frac{A}{N}\right)^2 \frac{(E_z^e)^3}{(\hbar s)^4} |\langle\downarrow j|I_+S_-|\uparrow i\rangle|^2 \\ &\quad \times \left\{\left[\frac{1}{\hbar\Omega_-}\left(1+\frac{E_z^e}{\hbar\Omega_-}\right) + \frac{1}{\hbar\Omega_+}\left(1-\frac{E_z^e}{\hbar\Omega_+}\right)\right]^2 \right. \\ &\quad \left. + \left[\frac{1}{\hbar\Omega_+}\left(1+\frac{E_z^e}{\hbar\Omega_+}\right) + \frac{1}{\hbar\Omega_-}\left(1-\frac{E_z^e}{\hbar\Omega_-}\right)\right]^2\right\}. \end{aligned}$$

The initial state is $|m\uparrow i\rangle$ and the final state is $|m\downarrow j\rangle$, where i and j represent nuclear spin eigenstates. m stands for the initial orbital state (QD s orbital). $\bar{n}_{q\nu}$ is the Bose-Einstein distribution for phonons with momentum q and phonon branch ν at temperature T. We consider both phonon absorption and emission processes, depending on the direction of the total magnetic field. $N_q = \bar{n}_{q\nu}$ for phonon emission processes while $N_q = \bar{n}_{q\nu} + 1$ for phonon absorption processes. $f_{def}(E_z^e)$ is obtained from the deformation potential term and $f_{piezo}(E_z^e)$ is obtained from the piezoelectric interaction. T_{ep} is the transition amplitude for the phonon-assisted spin-flip processes. Here the hyperfine interaction not only induces electron-nuclear spin flip flop but also mixes electron spin and orbital degrees of freedom.[54] The electron spin-up (-down) state in the m orbital is mixed with the electron spin-down (-up) state from a higher orbital state l. E_m and E_l represent the energies of the m and l Fock-Darwin orbital states. For simplicity, we only consider the phonon emission/absorption between s orbital and p orbital states (we do not anticipate the inclusion of contributions from higher orbital states to qualitatively alter our results). Ξ is the deformation potential constant. The piezoelectric constant is denoted as $ee_{14} = 2 \times 10^{-10}$ J/m, sound speed: $s = 3 \times 10^3$ m/s, electron density in InAs: $\rho = 5.7 \times 10^3$ Kg/m^3. In the presence of an external magnetic field, Fock-Darwin energy levels can be represented as $\hbar\Omega_{\pm} = \hbar\Omega \pm \hbar\omega_c/2$, where $\hbar\Omega$ is the electronic confinement in the QD and is about 30 meV in the type of QD we consider. The cyclotron frequency is $\omega_c = eB/m^*$, where $m^* = 0.023 m_0$ is the effective electron mass in the InAs QDs. l_0 is the lateral dimension of the QD. The transition rate due to the deformation potential is proportional to the fifth power of the electronic Zeeman splitting while the contribution from the piezoelectric interaction is proportional to the third power of the electronic Zeeman spitting.

3. Strain-induced depolarization

Due to the strain-induced quadrupole interaction, where the principal axis Z is generally not parallel to the external field direction z, the nuclear spin eigenstates are a mixture of I_z eigenstates. This means that the nonflip-flop term in Eq. (5), $I_z^k S_z$, can now induce transitions between different nuclear spin states and cause NSP (see red two-way arrows in Fig. 5). Since the energy transfer between these nuclear spin states is generally much less than cotunneling energy [0.033 μeV (Ref. 48)], this process is not limited by energy conservation considerations. These depolarization rates can be calculated by the Fermi's golden rule,

$$F_{ij} = \left(\frac{A_{\mathrm{As}}}{N}\right)^2 \frac{2\tau_c f_e |\langle i|I_z|j\rangle|^2}{\hbar^2 + \tau_c^2 (E_i^n - E_j^n)^2}, \tag{7}$$

where i and j represent nuclear spin eigenstates, and E_i^n and E_j^n stand for the nuclear spin eigenenergies.

D. Master equation of population

Depending on the helicity of the excitation photon (σ^+/σ^-), the electron can pump nuclear spins either to the higher-energy spin states or the lower-energy states. Take, for example, nuclear spins being pumped to the highest-energy nuclear spin state, as shown in Fig. 5, the average NSP can be evaluated by the master equation of population [see Eq. (8)],[2] which is determined by the balance between the pumping and depolarization channels,

$$\frac{dp_i}{dt} = \sum_{j \neq i} W_{j,i} p_j - \sum_{j \neq i} W_{i,j} p_i, \tag{8}$$

where $W_{j,i} \neq W_{i,j}$ represents the total transition rate between the i and j states, and p_i represents the nuclear spin population at ith state with $i = 1, 2, 3, 4$,

$$\frac{d}{dt}\begin{bmatrix} p_1 \\ p_2 \\ p_3 \\ p_4 \end{bmatrix} = M \begin{bmatrix} p_1 \\ p_2 \\ p_3 \\ p_4 \end{bmatrix},$$

where

$$M = \begin{bmatrix} -(F_{12}+F_{13}+F_{14}) & (D'_{12}+F_{12}) & F_{13} & F_{14} \\ F_{12} & -(D'_{12}+F_{12}+F_{23}+F_{24}) & (F_{23}+D'_{23}) & F_{24} \\ F_{13} & F_{23} & -(D'_{23}+F_{23}+F_{34}+F_{13}) & (D'_{34}+F_{34}) \\ F_{14} & F_{24} & F_{34} & -(D'_{34}+F_{34}+F_{24}+F_{14}) \end{bmatrix}.$$

Here $D'_{ij} = D_{ij} + \Gamma_{ij}$ is the total pumping rate. The system is highly nonlinear due to the population dependence of the pumping rate. The steady-state nuclear spin polarization $\langle I_z \rangle = \Sigma_i p_i \langle I_i \rangle$ has to be calculated self-consistently.

IV. RESULTS OF NUCLEAR SPIN POLARIZATION

Recent experiments have achieved NSP in $\mathrm{In}_x\mathrm{Ga}_{1-x}\mathrm{As}$ QDs at various magnetic fields. NSP of 10–20 % is created in $\mathrm{In}_{0.9}\mathrm{Ga}_{0.1}\mathrm{As}$ QDs at below 1 T,[23] 40% in $\mathrm{In}_{0.6}\mathrm{Ga}_{0.4}\mathrm{As}$ at approximately 2 T,[28,29] and 80% in $\mathrm{In}_{0.9}\mathrm{Ga}_{0.1}\mathrm{As}$ at 5 T.[30] To better understand the differences in these results, we calculate the NSP in $\mathrm{In}_{0.25}\mathrm{Ga}_{0.75}\mathrm{As}$ (QD1), $\mathrm{In}_{0.6}\mathrm{Ga}_{0.4}\mathrm{As}$ (QD2), and $\mathrm{In}_{0.9}\mathrm{Ga}_{0.1}\mathrm{As}$ (QD3) quantum dots at various magnetic fields. The default temperature for our calculations is 4 K, unless otherwise identified.

The Z component strain tensor e_{ZZ} is a good indication of strain strength in our simplified model of the QD. As shown

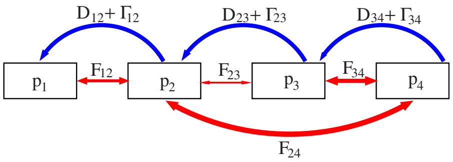

FIG. 6. (Color online) Sketch of possible transitions between nuclear spin states. The blue one-way arrows represent the pumping channels and the red two-way arrows represent the depolarization channels. The thickness of the arrows qualitatively represents the strength of the corresponding transition.

in Fig. 1, the largest electric field gradient is V_{ZZ}, which is proportional to e_{ZZ}. Near the surface of a pancakelike pure InAs QD embedded in GaAs, e_{ZZ} ranges between 4–8 %.[32,38,39,42] Inside, the strain is distributed more or less evenly, and e_{ZZ} is 3.5%, which is about half of the lattice mismatch between InAs and GaAs (7%). To give a quantitative estimate, we assume that the strain information is completely contained in the e_{ZZ} tensor element, which reflects the calculated lattice mismatch in dots with $\mathrm{In}_x\mathrm{Ga}_{1-x}\mathrm{As}$ compositions.[55] By interpolation, we estimate e_{ZZ} in QD1, QD2, and QD3 to be 2.5%, 4.3%, and 6.3%, respectively.

It is worth noting that the electron g factor in a $\mathrm{In}_x\mathrm{Ga}_{1-x}\mathrm{As}$ self-assembled quantum dot depends on the strain strength.[56] Based on the g factors given in experiments,[28,51,57] we take the g factors in QD1, QD2, and QD3 to be −0.6, −0.7, and −0.8, respectively.

A. Single arsenic nuclear spin polarization

To understand nuclear spin polarization in different compositions of $\mathrm{In}_x\mathrm{Ga}_{1-x}\mathrm{As}$ quantum dots, we first start with the nuclear spin polarization of As. The simplest case is the high magnetic field region, as shown in Fig. 3(d), where the nuclear spin Zeeman energy is much larger than the quadrupole splitting. Here nuclear spin eigenstates are close to the eigenstates of I_z so that $\langle i|I_z|j\rangle \approx 0$. Accordingly, the depolarization rates [see Eq. (7)] between nuclear spin states are approximately zero. Therefore nuclear spins can be pumped to the highest nuclear spin state and nearly full nuclear spin polarization can be obtained.

In low to intermediate field regions, the calculation for NSP becomes more complicated since the mixing between different nuclear spin Zeeman states become stronger than the higher-field case. The physical picture of various possible transitions is given in Fig. 6.

According to Fig. 6, in the absence of all the depolarization channels, nuclear spins can always be pumped to the highest spin state, and thus full NSP can be obtained. In the absence of F_{12}, no matter how strong other depolarization channels (F_{23}, F_{24}, and F_{34}) are, the nuclear spins can still be pumped to state 1 eventually, and thus become fully polarized. Once F_{12} is turned on, and in combination with F_{23} or F_{24}, the pumped nuclear spins in state 1 can now leak back to state 3 or 4, and full polarization cannot be achieved. In other words, F_{12} is the key to depolarization. As an example, we plot all the depolarization rates and pumping rates in Fig. 7.

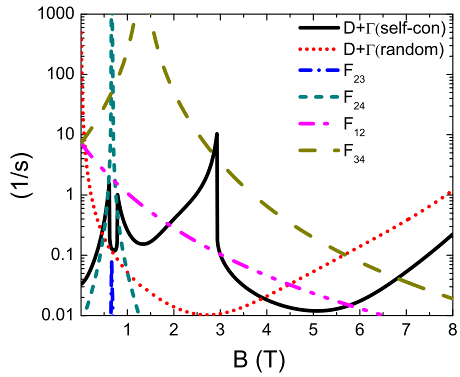

FIG. 7. (Color online) An example of pumping and depolarization rates in QD3. F_{13} and F_{14} do not appear here since they are smaller than 10^{-5}/s. The state 2–4 degeneracy (where the nuclear Zeeman and quadrupole splittings coincide) occurs at approximately 0.67 T, where F_{24} and F_{23} reach their peaks. The pumping rates $D+\Gamma$ (self-consistently) are calculated to self-consistency. In other words, these are pumping rates when nuclear polarization is already built up. $D+\Gamma$ (random) are the initial pumping rates with a random distribution of nuclear spins before the Overhauser field builds up.

In the two limits where $E_z^n > E_Q$ and $E_z^n < E_Q$, the state spectrum is mostly Zeeman type [Fig. 3(d)] or quadrupole-like [Fig. 3(a)]. In these cases F_{23} and F_{24} are very small compared to F_{12} (see Fig. 7) so that populations pumped into states 1 and 2 cannot leak to states 3 and 4. We can now simplify the four-level problem to a two-level problem, and find the steady-state solution from the following equations:

$$\dot{p}_1 = -F_{12}p_1 + (D_{12} + \Gamma_{12} + F_{12})p_2 = 0,$$

$$p_1 + p_2 = 1.$$

When $E_z^n < E_Q$, the cotunneling-assisted spin-flip transition D_{12} dominates, while when $E_z^n > E_Q$ the phonon-assisted spin-flip transition Γ_{12} is dominant, especially above 5 T (see Fig. 4). At fields lower than approximately 5 T, the average nuclear spin polarization can be expressed as follows:

$$\langle I_z \rangle \approx \frac{1}{2} + \cfrac{1}{1 + \cfrac{F_{12}}{D_{12} + F_{12}}} \tag{9}$$

while at higher fields

$$\langle I_z \rangle \approx \frac{1}{2} + \cfrac{1}{1 + \cfrac{F_{12}}{\Gamma_{12} + F_{12}}}. \tag{10}$$

From Eqs. (3) and (7), when $E_z^n > E_Q$, F_{12} is approximately

$$F_{12} = \left(\frac{A_{\mathrm{As}}}{N}\right)^2 \frac{6\tau_c f_e \theta^2 \left(\dfrac{E_Q}{E_z^n}\right)^2}{\hbar^2 + \tau_c^2 (E_z^n)^2},$$

and when $E_z^n < E_Q$,

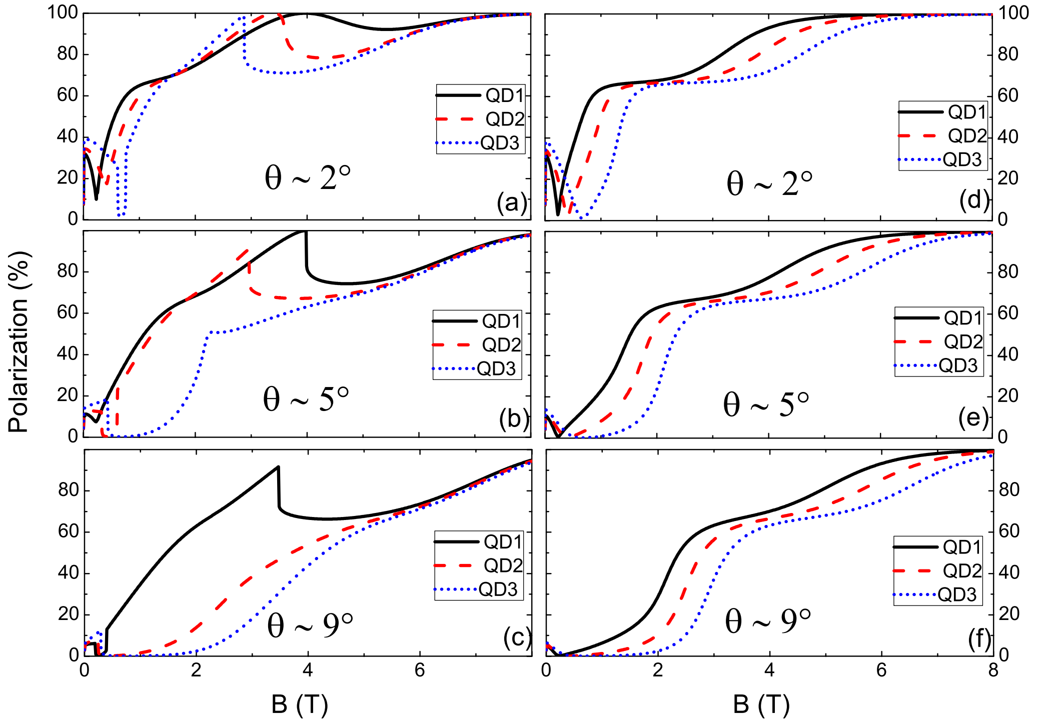

FIG. 8. (Color online) Nuclear spin polarization of As in three different $\mathrm{In}_x\mathrm{Ga}_{1-x}\mathrm{As}$ quantum dots, QD1, QD2, and QD3. The strain strengths in the dots are approximately proportional to the In concentration x. The solid, dashed, and dotted lines stand for the NSP in QD1, QD2, and QD3 with $x=0.25$, 0.6, and 0.9 respectively. θ represents the angle between the field gradient and the external magnetic field (the z axis). Here $\theta=2°$, 5°, and 9° are considered. Panels (a)–(c) show As nuclear spin polarizations at various strain conditions when the Overhauser field is antiparallel to the external magnetic field. Panels (d)–(f) show the parallel case. Overall, stronger strain or greater angle between the field gradient and growth direction suppresses the nuclear spin polarization.

$$F_{12}=\left(\frac{A_{\mathrm{As}}}{N}\right)^2\frac{6\tau_c f_e\theta^2}{\hbar^2+\tau_c^2(E_z^n)^2}.$$

Equations (9) and (13) can give a very good qualitative explanation to our calculations. At around 1.5–2 T, as shown in Figs. 8(a) and 8(d), D_{12} is at least one order of magnitude smaller than F_{12}, and the resulting $\langle I_z\rangle$ from Eq. (9) is ~ 1 (NSP is 67%), and is independent of field gradients of different angles and strengths (which determine F_{12}).

There are some general trends in the NSP as evident in Eq. (9) (we focus on the regime of $B<5$ T for our qualitative discussion in the following paragraph), where $\langle I_z\rangle$ depends only on the ratio of depolarization to polarization F_{12}/D_{12},

$$\langle I_z\rangle \approx \frac{1}{2}+\frac{1}{1+\dfrac{F_{12}/D_{12}}{1+F_{12}/D_{12}}}.$$

For $E_z^n>E_Q$,

$$\frac{F_{12}}{D_{12}}=\frac{\theta^2\left(\dfrac{E_Q}{E_z^n}\right)^2\left[\left(\dfrac{\hbar}{\tau_c}\right)^2+(-g^*\mu_B B_z+\delta_n)^2\right]}{\left[\left(\dfrac{\hbar}{\tau_c}\right)^2+(E_z^n)^2\right]}, \tag{11}$$

and for $E_z^n<E_Q$,

$$\frac{F_{12}}{D_{12}}\approx\frac{\theta^2\left[\left(\dfrac{\hbar}{\tau_c}\right)^2+(-g^*\mu_B B_z+\delta_n)^2\right]}{\left(\dfrac{\hbar}{\tau_c}\right)^2}. \tag{12}$$

Notice that for $E_z^n>E_Q$ the ratio F_{12}/D_{12} is proportional to the square of E_Q/E_z^n and θ. When E_Q or θ increases, F_{12}/D_{12} increases, and the average NSP $\langle I_z\rangle$ will decrease. This is illustrated in the overall trends of Fig. 8. Likewise, in the regime of $E_z^n<E_Q$, the ratio F_{12}/D_{12} is proportional to θ^2 and is a function of τ_c. Now when θ increases, $\langle I_z\rangle$ decreases, again shown in Fig. 8. Furthermore, when the second term of Eq. (12) is greater than the first (i.e., the electronic Zeeman energy is greater than the cotunneling energy), $F_{12}/D_{12}\propto\tau_c^2$, so that $\langle I_z\rangle$ decreases when τ_c increases. As shown in Fig. 9, the decrease in the cotunneling time constant (τ_c) enhances the overlap of the electronic energy levels, and increases the cross section of the hyperfine flip-flop processes. Therefore the resulting NSP increases, as shown in Fig. 9.

The nonlinear nature of our system becomes most prominent when the Overhauser field is antiparallel to the external magnetic field, as shown in Figs. 8(a)–8(c). Especially when the Overhauser field cancels out the external magnetic field (i.e., $2A\langle I_z\rangle_{max}\approx g^*\mu_B B_{ext}$) in D_{12}, as shown, for example, in Fig. 10(b). At this point the spin pumping rate D_{12} reaches its maximum, which leads to the peaks around 3–4 T in Fig. 8. The peak nuclear spin polarization is

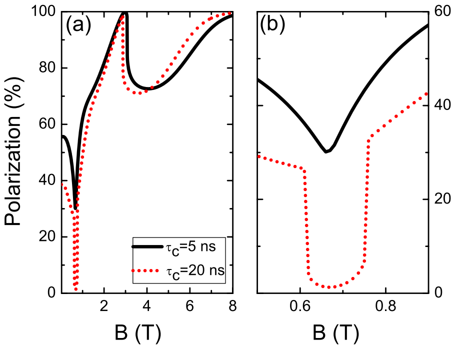

FIG. 9. (Color online) Field dependence of As nuclear spin polarization at different cotunneling rates. As shown in panel (a), the decrease in the cotunneling time constant (τ_c), or the increase in the cotunneling energy, enhances the overlap of the electronic energy levels, specifically when the external magnetic field is below approximately 5 T. The cross section of the hyperfine flip-flop processes is increased and the resulting nuclear spin polarization increases accordingly. Panel (b) is a zoom-in of panel (a) near the 2–4 degeneracy.

$$\langle I_z\rangle_{max} \approx \frac{1}{2} + \frac{1}{1 + \frac{\theta^2\left(\frac{E_Q}{E_z^n}\right)^2\left(\frac{\hbar}{\tau_c}\right)^2}{\left[\left(\frac{\hbar}{\tau_c}\right)^2+(E_z^n)^2\right]}} \approx \frac{g^*\mu_B}{2A}B_{ext}.$$

Therefore, when E_Q increases, the peak polarization $\langle I_z\rangle_{max}$ decreases. The corresponding external field B_{ext} decreases as well but that relationship is more complicated because E_z^n also depends on B_{ext}.

Equation (9) generally fits well with our numerical calculations, except for the case when the nuclear Zeeman energy is equal to the quadrupole energy. When the nuclear Zeeman energy is nearly resonant with the quadrupole energy, the nuclear spin polarization is harder to build up because the degeneracy between states 2 and 4 [see Fig. 3(b)] causes a maximum in the depolarization rate F_{24}, which is orders of magnitude larger than all other transition rates. The presence of this large transition rate equalizes the populations of states 2 and 4: $p_2=p_4$. Furthermore, in combination with F_{12}, it also prevents the nuclear spins from accumulating in the highest nuclear spin state. By setting up the master equation of Eq. (8), we find the steady-state solution from the following equations:

$$F_{12}p_1 = (D_{12} + F_{12})p_2,$$

$$p_3 \approx p_4,$$

$$p_1 + p_2 + p_3 + p_4 = 1.$$

The average NSP is

$$\langle I_z\rangle = \sum_i p_i\langle I_i\rangle$$

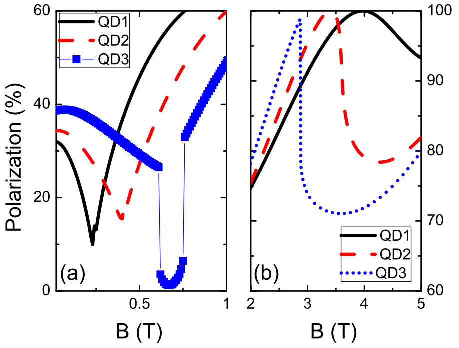

FIG. 10. (Color online) The As nuclear spin polarization near 2–4 degeneracy [panel (a)] and near the peak polarization [panel (b)]. The two panels are detailed views of Fig. 8(a) in these two regions. Near 2–4 degeneracy NSP depends on the ratio F_{12}/D_{12}, as shown in Eq. (10). In QD1 and QD2, $F_{12}/D_{12} \sim 1$, and the NSP is above 10% even at the degeneracy point. In QD3, $F_{12}/D_{12} \gg 1$, NSP is suppressed at the degeneracy and the field dependence of NSP becomes abrupt. The NSP peaks in panel (b) around 3–4 T occur when the Overhauser field cancels out the external magnetic field. These peaks shift to the lower magnetic field and lower nuclear polarization in stronger strain (see detail in text).

$$\approx \frac{3}{2}\frac{1}{1 + 4\left(\frac{F_{12}}{D_{12}}\right)}, \tag{13}$$

where

$$F_{12} = \left(\frac{A_{\mathrm{As}}}{N}\right)^2 \frac{6\tau_c f_e \theta^2}{\hbar^2 + \tau_c^2 E_Q^2}.$$

The achievable NSP at the 2–4 degeneracy point depends on the relative direction of the Overhauser field and the external magnetic field. When they are parallel, D_{12} is at least one order of magnitude smaller than F_{12}, thus the NSP at this degeneracy is only a few percent, as shown in Figs. 8(d)–8(f). When the fields are antiparallel, D_{12} may become comparable to F_{12}, and the resulting NSP strongly depends on the ratio of F_{12} to D_{12}, as shown in Figs. 8(a)–8(c) and 10(a). If this ratio is closer to 1 (such as for QD1 and QD2), the resulting NSP could be as high as 20%, much higher than that is achievable in the parallel field case. On the other hand, if this ratio is far above 1 (in QD3), the resulting NSP is suppressed, as shown in Fig. 10(a), while the field dependence becomes abrupt.

In order to gain more understanding of the highly nonlinear behavior of DNSP in QD3, we examine the time evolution of D_{12} at three different energy detunings, δ_1, δ_2, and δ_3, away from the Zeeman-quadrupole resonance, as shown in Fig. 11. According to panel (b), when the pumping rate is high enough to overcome the depolarization, the Overhauser field starts to build up. When the Overhauser field cancels out the external magnetic field, the pumping rate reaches a maximum in the time evolution of the system [the spikes shown in Fig. 11(b)]. The Overhauser field quickly exceeds the external magnetic field, and then this pumping rate falls off to a steady value, in a short time correlated with the

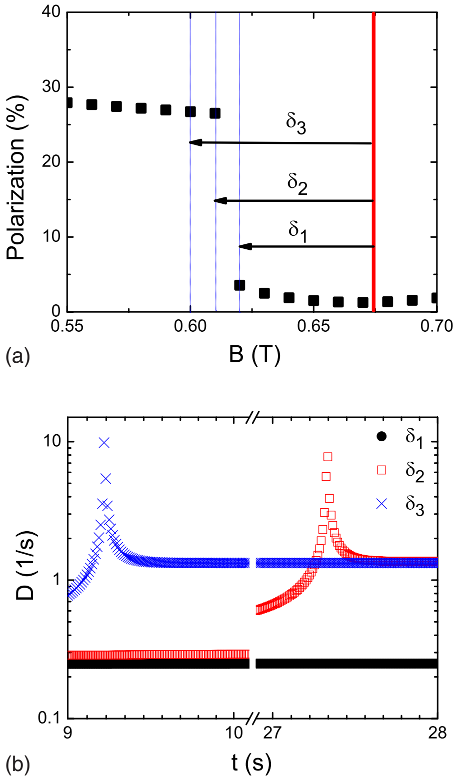

FIG. 11. (Color online) Time evolution of nuclear spin polarization rate [panel (b)] at different energy detunings [defined in panel (a)] in QD3 near the 2–4 degeneracy. The solid line at approximate 0.67 T in panel (a) stands for the 2–4 degeneracy, where As nuclear Zeeman energy is resonant with the quadrupole energy. δ_1, δ_2, and δ_3 are 1.7 neV, 1.75 neV, and 1.8 neV from this degeneracy, respectively. Panel (b) shows that NSP buildup time for δ_3 is approximately 30 and 10 s for δ_2. For δ_1, within our simulation time of 2000 s, the nuclear spin polarization is not built up. Clearly, as δ decreases, F_{24} gets closer to its maximum, which is orders of magnitude larger than all other rates, it takes longer and longer time to buildup the NSP, until it cannot be built up.

hyperfine energy, cotunneling time constant, and f_e. For δ_3, the NSP buildup time is approximately 10 s, and for δ_2 it is 30 s. For δ_1, the pumping never manages to overcome depolarization within our simulation time (2000 s), and the NSP is limited to a few percent. As the detuning δ approaches zero, F_{24} gets closer to its maximum, which is orders of magnitude larger than all other rates. In this regime, it takes longer and longer time to buildup the nuclear spin polarization, until it is practically impossible—beyond tens of seconds, nuclear spin relaxation channels that we do not consider, such as dipolar induced spin diffusion and direct spin-lattice relaxation, would have to be included for a complete physical picture to emerge.

When the nuclear Zeeman energy is equal to twice the quadrupole energy, nuclear spin states 3 and 4 are degenerate, as shown in Fig. 3(c). However, the NSP around this degeneracy is not as strongly affected as those near the 2–4 degeneracy. In this field region, F_{24} and F_{23} nearly vanish. The strong F_{34} equalizes the population of states 3 and 4, so that we can again isolate the four level problem to a two level one, and NSP can be calculated by using Eq. (9).

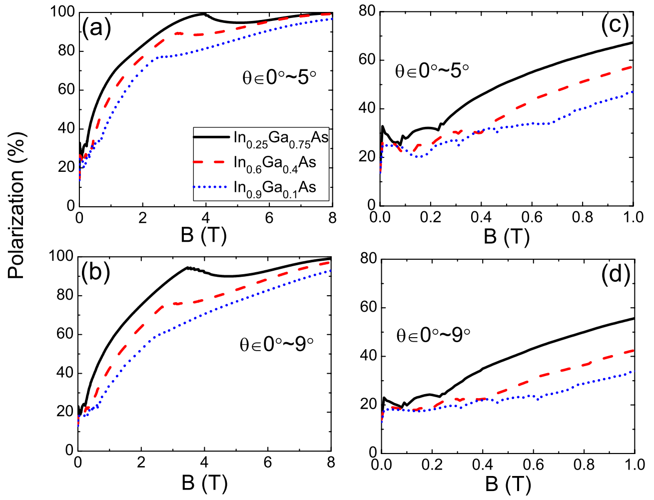

FIG. 12. (Color online) The nuclear spin polarization in $In_{0.25}Ga_{0.75}As$ (solid lines), $In_{0.6}Ga_{0.4}As$ (dashed lines), and $In_{0.9}Ga_{0.1}As$ (dotted lines) quantum dots. Panels (a) and (c) are for dots with $\theta \in 0-5°$ while panels (b) and (d) are for $\theta \in 0-9°$. Panels (c) and (d) are expansions of the low field regions of panels (a) and (b), respectively. (a) represents the nuclear spin polarization average over angles between 0°–5°. (b) represents the nuclear spin polarization average over angles between 0°–9°. (c) and (d) are the detail in low fields for (a) and (b), respectively. Comparing scales of panels (a) with (b), or (c) with (d), we note that stronger strain and larger variations in the direction of the field gradient suppress the nuclear spin polarization in low to intermediate fields.

B. Nuclear spin polarization in different compositions of $In_xGa_{1-x}As$ quantum dots

In all the NSP experiments in $In_xGa_{1-x}As$ QDs, the observable quantity is the total Overhauser field from all the nuclei of all the nuclear spin species. Since different nuclear isotopes have different gyromagnetic ratios (see Table I), and different nuclear spins generally experience different electric field gradients, the DNSP features we study in the previous section for a single nuclear spin species with a fixed quadrupole splitting would now occur in ranges of magnetic fields. The total effect is a superposition of contributions from all the individual ingredients. As we have discussed in Sec. III, we do not consider interactions between nuclear spins, whether they are of the same or different species.

To account for the distribution of strain in a QD, we assume a uniform distribution of angles between the electric field gradient and the applied magnetic field (which is along z direction as always). In Fig. 12, the angles between the electric field gradient and the external magnetic field are in the ranges of 0°–5° and 0°–9°. The peaks and dips in NSP of a single nuclear spin species, as shown in Fig. 8, are now smoothed out, as shown in Fig. 12.

Our results show a qualitative agreement with various experiments.[28,29,51] A high degree of nuclear spin polarization can be created in high-field regions while the polarization is limited in low-field regions. Overall the achievable nuclear spin polarization in $In_xGa_{1-x}As$ QDs is related to the concentration of indium and the resulting strain distribution in the dots. In general, stronger strain and larger angle be-

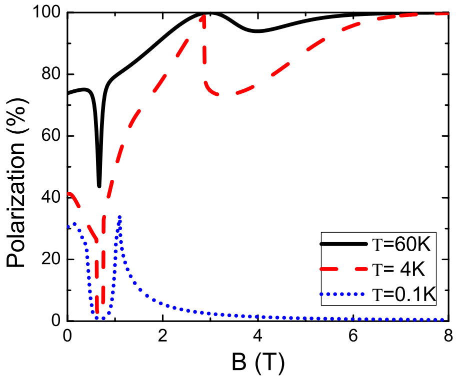

FIG. 13. (Color online) Temperature dependence of As nuclear spin polarization. The solid, dashed, and dotted lines stand for the nuclear spin polarization at temperatures of 0.1 K, 4 K, and 60 K respectively. The nuclear spin polarization is easier to buildup at higher temperature since the phonon population and cotunneling constants increase as temperature increases.

tween the field gradient and growth direction suppress the nuclear spin polarization.

V. DISCUSSION

In our calculations of nuclear spin polarization, the spin pumping is achieved by first optically orienting the electron spins, then transferring the electron spin polarization to the nuclear spins via either cotunneling-assisted processes or phonon-assisted processes. In the latter we have not included any spin mixing caused by spin-orbit interaction. However, it is well known that the spin-orbit interaction is quite strong in InAs dots.[58] Thus we have also explored how the spin-orbit interaction might take part in the DNSP.[59,60] More specifically, we have calculated the spin-flip transition rate from the combination of the hyperfine interaction, spin-orbit interaction, and the electron-phonon interaction, and we find the transition rate is linearly proportional to the electronic Zeeman splitting. Our results show that the inclusion of spin-orbit interaction into the spin-transfer process yields a slower process (by 2 orders of magnitude even at the relatively low magnetic field of 1 T) than the hyperfine interaction combined with electron-phonon interaction alone. Therefore, we exclude this mechanism from our current study.

Our calculations presented so far are done at $T=4$ K. We have also explored the temperature dependence of the As NSP in a QD. Both cotunneling and phonon emission/absorption (especially absorption) are affected by temperature changes, via Fermi level broadening and phonon populations, so that spin-flip rate will change accordingly. Consider, for example, nuclear spins being pumped to the highest-energy state at high fields, where spin transitions are assisted by phonon absorption, as shown in Fig. 5. We have calculated As NSP at three different temperatures: 0.1, 4, and 60 K. The results are shown in the high-field region of Fig. 13, where the NSP can be built up to larger values at temperature 60 K than 4 K and 0.1 K (especially at $B>5$ T), since at a fixed magnetic field the phonon population decreases as temperature decreases $[N\sim\frac{1}{\exp(E/k_BT)-1}]$. In the low-field region, the spin transition is assisted by cotunneling, and the cotunneling time constant τ_c is inversely proportional to the temperature.[48] Therefore the cotunneling-assisted processes are more efficient at higher temperatures,[61] as shown in Fig. 13. At present we do not have a clear analytical understanding of the abrupt change in NSP as shown in Fig. 11. We are currently working on a full density-matrix method that includes all the off-diagonal terms for the electron-nuclear spin system. Such a calculation could also help us ascertain the validity of the master equation approach we adopt in the present study.

VI. CONCLUSIONS

In summary, we have calculated nuclear spin polarization through optical orientation of electron spins in a self-assembled quantum dot. We have explored how NSP of a single nuclear species depends on the external magnetic field with various strain strengths, angles between the electric field gradient and the growth direction, and cotunneling energies. We show that, in high magnetic fields, higher degrees of NSP can be achieved, where the nuclear spin Zeeman energy is much larger than the quadrupole splitting. In this regime the nuclear spin eigenstates are close to the eigenstates of I_z so that the depolarization rates between nuclear spin states are approximately zero. Therefore nuclear spins can be pumped to the highest nuclear energy state without leaking back to lower-energy states. In low to intermediate field regions, NSP is strongly affected by the strain distribution. Generally speaking, in the same QD, the NSP is lower when the electric field gradient is at a larger angle from the external magnetic field, because strain along transverse directions (relative to the magnetic field) is the driving force behind depolarization transitions for the nuclear spins. In addition, NSP is lower at smaller cotunnelling rates (when, for example, the allowed electronic state in the QD is far below the Fermi sea). Furthermore, NSP is also harder to buildup in a QD with a larger magnitude of strain. Our calculation shows that higher strain strength in a QD leads to smaller NSP in general.

For NSP in $\mathrm{In}_x\mathrm{Ga}_{1-x}\mathrm{As}$ quantum dots, our results are obtained from incoherent superpositions of In, Ga, and As contributions in different proportions. We show that nearly full nuclear spin polarization can be created in high-field regions, while it is limited in low-field regions. Our results indicate that the concentration of indium and the resulting strain distribution in the dots play a crucial role in DNSP. For example, at low magnetic fields, nuclear spin polarization is harder to buildup in $\mathrm{In}_{0.9}\mathrm{Ga}_{0.1}\mathrm{As}$ than in $\mathrm{In}_{0.6}\mathrm{Ga}_{0.4}\mathrm{As}$. The interplay between the nuclear quadrupole interaction and Zeeman splitting could lead to suppression of nuclear spin polarization. Our results are in qualitative agreement with the measured nuclear spin polarization in the experimental work of various groups.[28–30,34,51]

Our results suggest that for a dot with a uniform strain distribution (and with a principal axis away from the external magnetic field), a minimum in NSP should be expected when the nuclear Zeeman energy is equal to the quadrupole energy. Moreover, a peak should be observed in the intermediate field regions (around 3–4 T), where the Overhauser field cancels out the external magnetic field.

ACKNOWLEDGMENTS

We thank financial support by NSA/LPS through ARO under Grants No. W911NF0610209 and No. W911NF0910393. X.H. also acknowledges supports by Joint Quantum Institute of University of Maryland and DARPA QuEST.

---

[1] C. Slichter, *Principles of Magnetic Resonance* (Springer-Verlag, Berlin, 1992).
[2] A. Abragam, *The Principles of Nuclear Magnetism* (Clarendon Press, Oxford, 1961).
[3] B. E. Kane, Nature (London) **393**, 133 (1998).
[4] J. M. Taylor, C. M. Marcus, and M. D. Lukin, Phys. Rev. Lett. **90**, 206803 (2003).
[5] D. Loss and D. P. DiVincenzo, Phys. Rev. A **57**, 120 (1998).
[6] I. A. Merkulov, A. L. Efros, and M. Rosen, Phys. Rev. B **65**, 205309 (2002).
[7] W. M. Witzel, R. de Sousa, and S. Das Sarma, Phys. Rev. B **72**, 161306(R) (2005).
[8] W. A. Coish and D. Loss, Phys. Rev. B **70**, 195340 (2004).
[9] W. Yao, R.-B. Liu, and L. J. Sham, Phys. Rev. B **74**, 195301 (2006).
[10] S. I. Erlingsson and Y. V. Nazarov, Phys. Rev. B **70**, 205327 (2004).
[11] A. V. Khaetskii, D. Loss, and L. Glazman, Phys. Rev. Lett. **88**, 186802 (2002).
[12] F. Dominguez and G. Platero, Phys. Rev. B **80**, 201301(R) (2009).
[13] G. Burkard, D. Loss, D. P. DiVincenzo, and J. A. Smolin, Phys. Rev. B **60**, 11404 (1999).
[14] D. Klauser, W. A. Coish, and D. Loss, Phys. Rev. B **73**, 205302 (2006).
[15] G. Ramon and X. Hu, Phys. Rev. B **75**, 161301(R) (2007).
[16] *Optical Orientation*, edited by F. Meier and B. Azkharchenya (North-Holland, Amsterdam, 1984).
[17] M. Dobers, K. v. Klitzing, J. Schneider, G. Weimann, and K. Ploog, Phys. Rev. Lett. **61**, 1650 (1988).
[18] B. E. Kane, L. N. Pfeiffer, and K. W. West, Phys. Rev. B **46**, 7264 (1992).
[19] J. H. Smet, R. A. Deutschmann, F. Ertl, W. Wegscheider, G. Abstreiter, and K. von Klitzing, Nature (London) **415**, 281 (2002).
[20] D. Gammon, E. S. Snow, B. V. Shanabrook, D. S. Katzer, and D. Park, Phys. Rev. Lett. **76**, 3005 (1996).
[21] K. Ono and S. Tarucha, Phys. Rev. Lett. **92**, 256803 (2004).
[22] J. Baugh, Y. Kitamura, K. Ono, and S. Tarucha, Phys. Rev. Lett. **99**, 096804 (2007).
[23] C. W. Lai, P. Maletinsky, A. Badolato, and A. Imamoglu, Phys. Rev. Lett. **96**, 167403 (2006).
[24] J. R. Petta, J. M. Taylor, A. C. Johnson, A. Yacoby, M. D. Lukin, C. M. Marcus, M. P. Hanson, and A. C. Gossard, Phys. Rev. Lett. **100**, 067601 (2008).
[25] J. Danon, I. T. Vink, F. H. L. Koppens, K. C. Nowack, L. M. K. Vandersypen, and Y. V. Nazarov, Phys. Rev. Lett. **103**, 046601 (2009).
[26] O. Krebs, P. Maletinsky, T. Amand, B. Urbaszek, A. Lemaitre, P. Voisin, X. Marie, and A. Imamoglu, Phys. Rev. Lett. **104**, 056603 (2010).
[27] P.-F. Braun, B. Urbaszek, T. Amand, X. Marie, O. Krebs, B. Eble, A. Lemaitre, and P. Voisin, Phys. Rev. B **74**, 245306 (2006).
[28] B. Eble, O. Krebs, A. Lemaitre, K. Kowalik, A. Kudelski, P. Voisin, B. Urbaszek, X. Marie, and T. Amand, Phys. Rev. B **74**, 081306(R) (2006).
[29] A. I. Tartakovskii, T. Wright, A. Russell, V. I. Fal'ko, A. B. Van'kov, J. Skiba-Szymanska, I. Drouzas, R. S. Kolodka, M. S. Skolnick, P. W. Fry, A. Tahraoui, H.-Y. Liu, and M. Hopkinson, Phys. Rev. Lett. **98**, 026806 (2007).
[30] P. Maletinsky, Ph.D. thesis, ETH, 2008.
[31] R. I. Dzhioev and V. L. Korenev, Phys. Rev. Lett. **99**, 037401 (2007).
[32] A. J. Williamson and A. Zunger, Phys. Rev. B **59**, 15819 (1999).
[33] D. Gammon, A. L. Efros, T. A. Kennedy, M. Rosen, D. S. Katzer, D. Park, S. W. Brown, V. L. Korenev, and I. A. Merkulov, Phys. Rev. Lett. **86**, 5176 (2001).
[34] A. S. Bracker *et al.*, Phys. Rev. Lett. **94**, 047402 (2005).
[35] R. K. Sundfors, Phys. Rev. B **10**, 4244 (1974).
[36] R. K. Sundfors, R. K. Tsui, and C. Schwab, Phys. Rev. B **13**, 4504 (1976).
[37] R. C. Weast, *Handbook of Chemistry and Physics* (The Chemical Rubber, Cleveland, OH, 2007).
[38] M. Grundmann, O. Stier, and D. Bimberg, Phys. Rev. B **52**, 11969 (1995).
[39] M. Korkusiński and P. Hawrylak, Phys. Rev. B **63**, 195311 (2001).
[40] O. Stier, M. Grundmann, and D. Bimberg, Phys. Rev. B **59**, 5688 (1999).
[41] W. Sheng and P. Hawrylak, Phys. Rev. B **72**, 035326 (2005).
[42] M. Yang, S. J. Xu, and J. Wang, Appl. Phys. Lett. **92**, 083112 (2008).
[43] D. Paget, T. Amand, and J.-P. Korb, Phys. Rev. B **77**, 245201 (2008).
[44] C. Deng and X. Hu, Phys. Rev. B **72**, 165333 (2005).
[45] E. Yusuf and X. Hu (unpublished).
[46] C. Deng and X. Hu, Phys. Rev. B **73**, 241303(R) (2006).
[47] L. Cywiński, W. M. Witzel, and S. Das Sarma, Phys. Rev. Lett. **102**, 057601 (2009).
[48] J. M. Smith, P. A. Dalgarno, R. J. Warburton, A. O. Govorov, K. Karrai, B. D. Gerardot, and P. M. Petroff, Phys. Rev. Lett. **94**, 197402 (2005).
[49] J. R. Schrieffer and P. A. Wolff, Phys. Rev. **149**, 491 (1966).
[50] G. Mahan, *Many Particle Physics* (Kluwer Academic/Plenum, New York, 2000).
[51] P. Maletinsky, A. Badolato, and A. Imamoglu, Phys. Rev. Lett. **99**, 056804 (2007).
[52] R. J. Warburton, C. Schaflein, D. Haft, F. Bickel, A. Lorke, K. Karrai, J. M. Garcia, W. Schoenfeld, and P. M. Petroff, Nature

(London) **405**, 926 (2000).

[53] J. Dreiser, M. Atature, C. Galland, T. Muller, A. Badolato, and A. Imamoglu, Phys. Rev. B **77**, 075317 (2008).

[54] S. I. Erlingsson and Y. V. Nazarov, Phys. Rev. B **66**, 155327 (2002).

[55] M. A. Migliorato, A. G. Cullis, M. Fearn, and J. H. Jefferson, Phys. Rev. B **65**, 115316 (2002).

[56] C. E. Pryor and M. E. Flatte, Phys. Rev. Lett. **96**, 026804 (2006).

[57] M. Bayer *et al.*, Phys. Rev. B **65**, 195315 (2002).

[58] R. Wingler, *Spin-Orbit Coupling Effects in Two-Dimensional Electron and Hole Systems* (Springer, Berlin/Heidelberg, 2003).

[59] M. Florescu and P. Hawrylak, Phys. Rev. B **73**, 045304 (2006).

[60] A. V. Khaetskii and Y. V. Nazarov, Phys. Rev. B **61**, 12639 (2000).

[61] B. Urbaszek, P.-F. Braun, T. Amand, O. Krebs, T. Belhadj, A. Lemaitre, P. Voisin, and X. Marie, Phys. Rev. B **76**, 201301(R) (2007).